energies

Article

Simulation of Micron and Submicron Particle Trapping by Single Droplets with Electrostatic Fields

Qiaoqun Sun [1], Wei Zhang [2], Yu Zhang [2,*], Yaodong Dan [3], Heming Dong [2], Jiwang Wen [2], Qian Du [2] and Jianmin Gao [2]

[1] School of Aerospace and Construction Engineering, Harbin Engineering University, Harbin 150001, China
[2] School of Energy Science and Engineering, Harbin Institute of Technology, Harbin 150001, China
[3] China Institute of Special Equipment Inspection, Beijing 100029, China
* Correspondence: zhang.y@hit.edu.cn

Abstract: Wet electrostatic precipitators have problems such as uneven water distribution and poor economy in applying ultra-clean particulate matter emissions from coal-fired boilers. Upgrading the droplets in wet dust removal to charged mobile collectors can effectively compensate for these shortcomings. In this paper, the effects of particle sphericity, particle size, and charge on the capture efficiency of a single droplet for capturing micron and submicron particles are qualitatively studied by simulating the process of particle capture by charged droplets in a turbulent flow field. The simulation results show that the trapping efficiency of charged droplets is positively correlated with the sphericity and the amount of charge. The particle size significantly impacts the capture efficiency, and the increase in size increases the capture efficiency, and the capture efficiency of 5.49 μm particles reaches 100%. The effect of particle movement speed on the capture efficiency needs to be considered in combination with particle size. For micron particles, the capture efficiency is close to 100% when the movement speed is 0.3 m/s and 0.5 m/s. For submicron particles, the aggregation morphology is lower at lower speeds. Simple non-spherical particles have greater capture efficiency.

Keywords: charged droplets; sphericity; numerical simulation; trapping efficiency

check for updates

Citation: Sun, Q.; Zhang, W.; Zhang, Y.; Dan, Y.; Dong, H.; Wen, J.; Du, Q.; Gao, J. Simulation of Micron and Submicron Particle Trapping by Single Droplets with Electrostatic Fields. *Energies* **2022**, *15*, 8487. https://doi.org/10.3390/en15228487

Academic Editor: Dumitran Laurentiu

Received: 18 October 2022
Accepted: 10 November 2022
Published: 14 November 2022

1. Introduction

With the massive consumption of coal, particulate matter emission severely impacts the environment. However, in recent years, China has experienced rapid industrialization and the electricity demand is still in the increasing stage. In particular, the production and operation of coal-fired power plants generate a large amount of particulate emissions. A large amount of particulate matter in their soot emissions can cause serious pollution to the environment and affect people's health. To control the environmental damage of particulate matter, waste gas generated in the industrial production process must be purified before being discharged into the atmosphere. The wet dust collector has a better effect than various dust removal technologies [1]. Wet electrocoagulation technology is widely used due to its advantages of low energy consumption, pressure reduction, and the ability to remove soluble gas, but it also has some shortcomings, such as serious corrosion and the easy formation of corona inhibition [2,3]. The study of particle capture by single droplet is the basis for improving wet electrocoagulation. Studying the capture of particles by single droplet can deeply understand and use the wet deposition mechanism in the atmospheric environment to remove particles [2].

At present, scholars have studied the particle capture process of charged single droplets, most of which are based on the assumption of spherical particles, and the research on non-spherical particles is still in the qualitative research stage. However, Jiang [4] and Yao [5] and other studies found that the shape of the particles affects the humidity and thus the charging capacity. If the particle shape is not considered, the charged single droplet captures the particles with a large deviation, so the particle shape affects the capture. The effect of efficiency cannot be ignored, and the "sphericity" of the particles is proposed as an important characteristic parameter [6]. Wadell [7] defined, by the ratio of the spherical particle surface area Av to the non-spherical surface area Ap with the same volume of non-spherical particles, a highly accurate relationship between sphericity and drag force established through experimental measurements.

According to the current research progress, the factors affecting the capture efficiency in the process of capturing particles by a single charged droplet are not only particle sphericity but also particle size, particle and droplet charge amount, and particle motion speed [8]. Zuo Ziwen [9] and others designed an experimental device for particle capture by charged droplets and found that the particle capture capacity of charged droplets was more than an order of magnitude higher than that of non-charged droplets, and the capture capacity of droplets was similar to that of non-charged droplets. The amount of charge is linearly proportional. Li Lin [10] conducted an experimental study on the process of electrostatic spraying to remove particulate matter from flue gas. The results show that electrostatic spraying has a significant effect on agglomerating particulate matter and small particles can aggregate to form larger particles, which improves the capture efficiency. Wang Junfeng and others [11] carried out an experiment of trapping particles by charged droplets. The research results show that charged droplets can capture more particles, and particles stay on the surface of the droplets due to surface tension, which affects the capture of the particles' set efficiency. Zuo and others [12] developed an experimental setup for trapping particles by charged droplets and studied the entire trapping process. The experimental results show that the number of particles captured by charged droplets is much larger than that of non-charged droplets, and the particles on the surface of charged droplets obviously aggregate together. Zhang Yaowen [13] developed an electrostatic spray cyclone dust removal system and carried out research on the influence of various factors on the dust reduction rate under different dust concentrations. The experimental results show that the increase in electric field strength is beneficial to improve the dust reduction rate of the device. In the thermo-dynamic characterization of free water and surface water of colloidal monomolecular polymeric particles using DSC, Peng Geng et al. [14] found that the effect of Manning condensation occurs when the charge on the surface of the particles is very high, and the effective charge density decreases, reducing the effective charge on its surface.

In terms of simulation, the core is the construction of the model and the definition of the capture efficiency. From the 2D model to the 3D model, the definition of the capture efficiency needs to be rewritten. In terms of numerical simulation, Wang [15], Shapiro and Laufer [16], and others found that if the droplets and particles are not charged or the charge is low, the particles can be driven to collide with the droplets by adding an electric field, but if the droplets and particles are two, all of them are charged, and the addition of an electric field weakens the capture of the particles by the droplets. Wang Junfeng [17] and Xie Liyu [18] carried out numerical simulation research on particles trapped by charged droplets. The research results show that when the direction of airflow movement and the direction of droplet deformation and projection are the same, although the collision efficiency is reduced, it can be improved and improve capture efficiency. Zhao Haibo and Zheng Chuguang [19–21] numerically simulated the process of removing boiler flue gas by electrostatic spraying, and discussed the effects of inertial collision, interception, Brownian diffusion, and electrostatic force on the capture efficiency. Wang Ao [22] used a three-dimensional model to study and considered the combined effect of inertial and thermophoretic mechanisms. The study found that in the range of the Reynolds number involved in spraying, the flow boundary layer near the droplets was separated and showed non-steady state and non-axisymmetric morphology. Based on the study of particle inertial motion behavior, Slinn and Davenport [23–26] established an inertial capture efficiency formula.

Weber et al. [27] studied the inertial trapping efficiency of droplets flowing around particles under the assumptions of the Stokes flow model and the potential flow model and estimated the inertial trapping efficiency at each Reynolds number (Re) between the two flow assumptions using the interpolation method, and the calculated results have a large deviation from the experimental and numerical simulation results. Bauer and others [28] assumed a steady-state axisymmetric flow field around the flow droplet and numerically simulated the inertial trapping of particles with St = 0.1 to 100 by the droplet at Re = 1 to 400. Slinn and others [25] fitted this numerical simulation result to obtain a formula for calculating inertial trapping efficiency at different Reynolds numbers (Re) and Stokes numbers (St), which is widely used to calculate inertial collision kernels to predict The removal coefficient of particulate matter during rainfall. The formula fitted by Slinn is in good agreement with the experimentally obtained efficiency in the range of Re < 300, but the relative deviation from the experimental data at higher Reynolds number (Re), such as in the study by Horn [29], is more than 20%.

To sum up, the research on wet electrocoagulation technology is extremely important, but the related analysis methods are not yet mature, and more in-depth research is needed. Therefore, a single droplet captures spherical and non-spherical particles under the action of an electrostatic field, which is simulated and studied to establish a numerical model and a physical model of the particle and study the particle size, particle charge, droplet charge, particle velocity, and particle size. Due to the effects of aggregation behavior and other factors on the capture efficiency, the research results are of great significance for improving the wet electrocoagulation technology and improving the particle capture efficiency.

2. Numerical Model

2.1. Force Analysis Equation

The main forces on the particles during their motion are shown in Table 1.

Table 1. Force analysis equations for particle motion.

Action Force	Force Analysis Equation	Serial Number
Gravity	$F_g = \frac{1}{6}\pi {d_p}^3 \rho_p g$	(1)
Buoyancy	$F_g = \frac{1}{6}\pi {d_p}^3 \rho g$	(2)
Inertial force	$F_g = -\frac{1}{6}\pi {d_p}^3 \rho_p \frac{\mathrm{du}_p}{d_t}$	(3)
Resistance force	$C_D = \frac{F_\gamma}{\pi {r_p}^2 \left[\frac{1}{2}\rho\left(u - {u_p}^2\right)\right]}$	(4)
	$F_r = \frac{\pi^2}{2} C_D \left\lvert u - u_\gamma \right\rvert (u - u_\gamma)$	(5)
Basset force	$F_B = \frac{3}{2} {d_\gamma}^2 \sqrt{\pi \rho \mu} \int\limits_{-\infty}^{t} \frac{\frac{du}{dt} - \frac{du_\gamma}{dt}}{\sqrt{t-\tau}} d\tau$	(6)
Saffman lift force	$F_s = 1.61(\mu\rho)^{\frac{1}{2}} d_\rho^2 (u - u_\rho) \left\lvert \frac{du}{dy} \right\rvert^{\frac{1}{2}}$	(7)
Additional mass force	$F_{VM} = \frac{1}{2}\rho V \left(\frac{du}{dt} - \frac{du_\rho}{dt}\right)$	(8)
Magnus lift force	$F_1 = \frac{1}{3}\pi {d^3}_p \rho u \varpi$	(9)

In addition to the main forces mentioned above, the traction forces on the particles should not be neglected. For the traction of spherical particles, the particle velocity (v) is the translational velocity of the particle center of mass, and the continuous fluid velocity (u) is usually defined in the region without particles. The continuous fluid velocity can also be extrapolated to the particle center of mass and expressed as $u_{@p}$, called the "unimpeded velocity." The relative velocity of particles (w) based on the "unobstructed velocity" can be expressed as [30]:

$$w(t) = v(t) - u_{@p}(t) \tag{10}$$

Assuming that the particle and fluid velocities are stable and uniformly distributed over the space away from the particles, $\nabla - u_{@p} = 0$ [31]. At this point, the magnitude of the trapping force is mainly determined by the particle Reynolds number (Rep).

$$\mathrm{Re}_{\rho} = \frac{\rho_f \left| w \right| d}{\mu_g} \tag{11}$$

where d denotes the particle diameter, ρ_f denotes the fluid density, and μ_f denotes the fluid viscosity. Nedelcu [32] derived the trajectory of spherical particles under the condition that the convection term (Rep $\ll$ 1) can be neglected:

$$F_D = -3\pi d \mu_f w \tag{12}$$

When the particle Reynolds number increases, the flow behind the particle is initially an attached laminar flow with Rep < 22, then a separate laminar flow zone, which becomes an unstable transition zone at 22 < Rep < 130, and then a turbulent zone at 130 < Rep < 1000 [31–35]. At 2000 < Rep < 300,000, the boundary layer starting in front of the particles ($\theta = 0°$) is laminar and separates at about 80° [35], creating a fully turbulent wake behind the particles. The total drag force is defined according to the drag coefficient (CD) as:

$$F_D = -\frac{\pi}{8} d^2 \rho_f C_D w w \tag{13}$$

For smaller values of Rep, the Stokes traction equation is appropriate. The traction coefficient (CD) measured in the range 2000 < Rep < 300,000 is almost constant, from about 0.4 to 0.45, which is also commonly referred to as the “Newtonian zone” [36]. The Stokes correction can be obtained by normalizing the traction by the creep flow solution.

$$f_{\mathrm{Re}} = \frac{F_D(\mathrm{Re}_\gamma)}{F_D(\mathrm{Re}_\gamma \to 0)} = \frac{C_D(\mathrm{Re}_\gamma)}{24/\mathrm{Re}_\gamma} \tag{14}$$

Equation (14) is uniform for Rep $\ll$ 1 and is proportional to Newton’s law for Rep (about 3000 < Rep < 200,000). A transition occurs in between due to the appearance and growth of the wake separation bubble [35].

An empirical formula including a traction coefficient can be derived from a series of assumptions. An empirical curve consisting of 10 components was given by Clift et al. [37] for extending the study of spheres to Rep as 106. The Stokes correction in this calculation gives

$$f_{\mathrm{Re}} = 1 + 0.15{\mathrm{Re}_\gamma}^{0.687} \quad \text{for Rer } < \ 800 \tag{15}$$

Regularly shaped non-spherical particles do not have an analytical solution for the trajectory even in creeping flows with large flow velocities; their shape and the corresponding correction for the trajectory can be approximated as ellipsoids by determining the effective aspect ratio (E). As shown in Figure 1, the cylinder can also be corrected for shape (fshape) to maintain sufficient accuracy [38–40]. As with the sphere shape factor, fshape is inversely proportional to the change in terminal velocity (for d = constant), as the trajectory correlation is linear in creeping flows.

$$f_{shape} = \frac{C_{D,shape}}{C_{D,shaere}}\bigg|_{\mathrm{Re} \ll 1 \& const.wol} = \frac{W_{term,sphere}}{W_{term,sphape}} \tag{16}$$

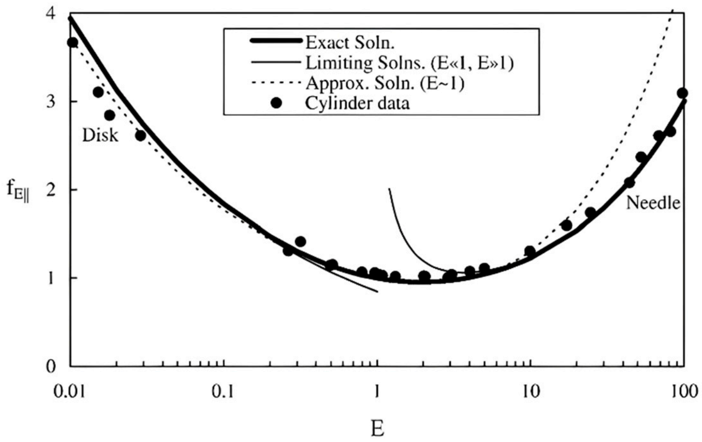

Figure 1. Effect of eccentricity on sphere trajectory correction [28].

In order to estimate the shape factor of non-spherical regular particles, two dimensionless area parameters, the surface area ratio and the projected area ratio, are usually considered [30]:

$$A^*_{surf} = \frac{A_{surf}}{\pi l^2}, A^*_{proj} = \frac{A_{proj}}{\frac{1}{4}\pi l^2} \tag{17}$$

The surface area ratio and the projected area ratio are usually considered. The surface area ratio is always greater than 1, i.e., $A^*_{surf} \geq 1$. The reciprocal of the surface area ratio is more commonly defined as the "sphericity ratio" [7], "sphericity" [24] or "shape factor". For cylinders with length-to-diameter ratio (Acyl), ratio (Acyl), the surface area ratio and equivalent volume diameter can be determined from geometric relationships [30]:

$$E_{cyl} = \frac{L_{cyl}}{d_{cyl}}, A^*_{surf} = \frac{2E_{cyl}+1}{(18E^2_{cyl})^{\frac{1}{3}}}, d = d_{cyl}\left(\frac{3E_{cyl}}{2}\right)^{\frac{1}{3}} \tag{18}$$

The projection area ratio depends mainly on the direction of projection of the particles and their shape. Under non-isometric conditions, Clift et al. [38] gave the A^*_{surf} and A^*_{proj} equations for biconical and rectangular equations. Although there are other ways to describe the non-spherical properties of particles, these are the two most commonly used parameters for symmetric particles, and both are also the most effective in correlating the traction [25,37].

Leith [41] proposed a correlation between the Stokes shape correction factor and these two area ratios:

$$f_{shape} = \frac{1}{3}\sqrt{A^*_{porj}} + \frac{2}{3}\sqrt{A^*_{surf}} \text{ for Rep } \ll 1 \tag{19}$$

From Equation (19), 1/3 of the sphere resistance is shape resistance (related to the projected area), 2/3 is friction resistance (related to the surface area), and the shape resistance and friction resistance are proportional to the particle size. A review by Ganser [39] shows that if the surface area ratio of a particle can be reasonably made to approach that of a sphere, the following relation can be used for a given aspect ratio.

$$\begin{gathered} A^*_{surf} = \frac{E^{\frac{-2}{3}}}{2} + \frac{E^{\frac{4}{3}}}{4\sqrt{1-E^2}} \ln\left(\frac{1+\sqrt{1-E^2}}{1-\sqrt{1-E^2}}\right) \\ A^*_{surf} = \frac{1}{2E^{\frac{2}{3}}} + \frac{E^{\frac{1}{3}}}{2\sqrt{1-E^{-2}}} \sin^{-1}\left(\frac{1+\sqrt{1-E^2}}{1-\sqrt{1-E^2}}\right) \end{gathered} \tag{20}$$

2.2. Governing Equation

2.2.1. Drag Equation

The trajectory of the particles in the vicinity of the adsorbed droplet is determined by Newton's equation [42].

$$m\frac{d\vec{w}}{dt} = \frac{C_d \mathrm{Re}_p}{24}\vec{F_r} + \vec{F_\tau} + \vec{F_g} \tag{21}$$

where w represents particle velocity, m represents particle mass, C_d represents traction coefficient, Re_p represents particle Reynolds number, F_r represents drag, F_g represents gravity, and F_ε represents electrostatic force.

Although the forces on the particles change during their motion and their trajectory changes, the whole physical process still follows the conservation of mass, momentum, and energy. The conservation of mass equation [43]:

$$\frac{\partial\rho}{\partial t} + \frac{\partial(\rho v_x)}{\partial x} + \frac{\partial(\rho v_y)}{\partial y} + \frac{\partial(\rho v_z)}{\partial z} = 0 \tag{22}$$

Conservation of momentum equation.

$$\frac{\partial(\rho v_x)}{\partial t} + div(\rho v_x v) = \frac{\partial\rho}{\partial t} + \frac{\partial\tau_{xx}}{\partial x} + \frac{\partial\tau_{yx}}{\partial y} + \frac{\partial\tau_{zx}}{\partial z} + F_x \tag{23}$$

$$\frac{\partial(\rho v_y)}{\partial t} + div(\rho v_y v) = \frac{\partial\rho}{\partial y} + \frac{\partial\tau_{xy}}{\partial x} + \frac{\partial\tau_{yy}}{\partial y} + \frac{\partial\tau_{zy}}{\partial z} + F_y \tag{24}$$

$$\frac{\partial(\rho v_z)}{\partial t} + div(\rho v_z v) = \frac{\partial\rho}{\partial z} + \frac{\partial\tau_{xz}}{\partial x} + \frac{\partial\tau_{yz}}{\partial y} + \frac{\partial\tau_{zz}}{\partial z} + F_z \tag{25}$$

Conservation of energy equation.

$$\frac{\partial}{\partial t}(\rho h) + div(phu) = div[(k+k_i)divT] + S_k \tag{26}$$

2.2.2. Capture Efficiency

The trapping efficiency of a moving particle in a laminar flow varies depending on the position of release. Here, by denoting y_0 as the maximum value of the trajectory of the trapped particles, the trapping efficiency can be defined as [44]:

$$E_T(d_d, d_p) = \frac{N}{N_0} = \left(\frac{2y_0}{d_d}\right)^2 \tag{27}$$

where d_d denotes droplet diameter, d_p denotes particle diameter, N denotes the number of particles trapped and N_0 denotes the number of particles released over the projected area of the droplet.

In turbulent flow, the flow field is unstable and the trajectory of motion is not unique. For this reason, the collision probability $\mathrm{e(d_d,d_p,Y)}$ is proposed to characterize the collision of particles with droplets under turbulent conditions. For simple micron spherical particle capture, the effect of each factor on the capture efficiency can be obtained by modelling the probability of collision for a given position.

The complexity of turbulent pulsations can be found from Figure 2, the previously defined trapping efficiency Equation (27) is not applicable to turbulent flows [45]. As the relative position of the particles, Y, affects the collision efficiency, the trapping efficiency can be synthesized by fitting the collision probability, as shown in Figure 3.

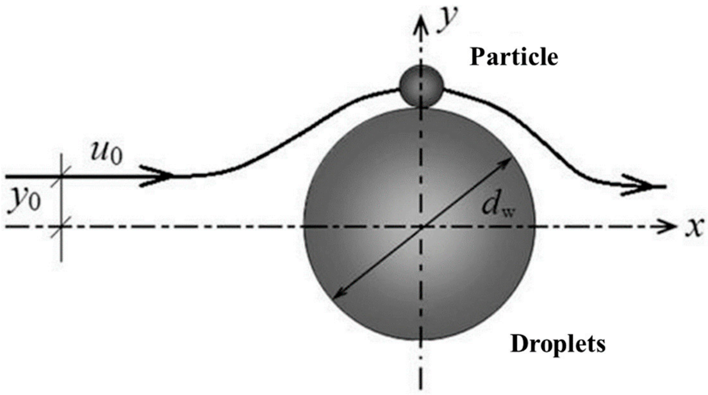

Figure 2. Schematic diagram of droplet trapping particles [44].

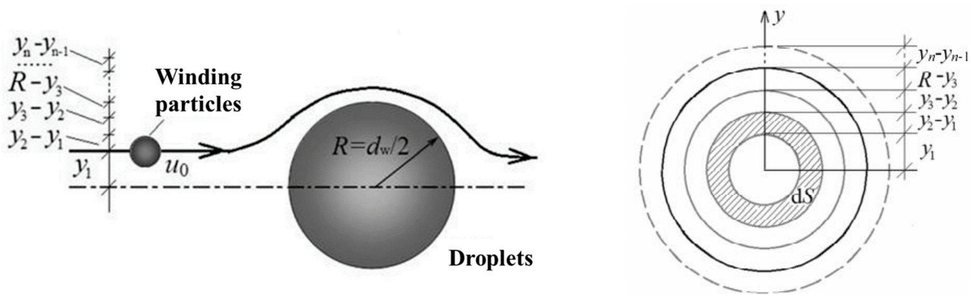

(**a**) Plan (**b**) Side view

Figure 3. Schematic diagram of turbulence fitting efficiency [44].

We can define the trapping efficiency η_s of droplet trapping particles as [44]

$$\begin{aligned}\eta_s &= \int_0^R e(d_d, d_p, Y)\left[\pi(y+dy)^2 - \pi y^2\right]/\pi R^2 \\ &= \int_0^R 2\pi e(d_d, d_p, Y) y dy/\pi R^2\end{aligned} \tag{28}$$

For ease of fitting, the above equation can be expanded as

$$\begin{aligned}\eta_\text{s} &= \sum_{n-1}^{n} e_n \pi\left(y_n^2 - y_{n-1}^2\right)/\pi R^2 \\ &= \left[y_1^2 e_1 + \left(y_2^2 - y_1^2\right)e_2 + \ldots + \left(y_n^2 - y_{n-1}^2\right)e_n\right]/R^2\end{aligned} \tag{29}$$

where y_1, y_2 … y_n are the 1st, 2nd … n outer circle radii of the micro-element circle, e_1, e_2 … e_n are the collision efficiencies of the released particles at the corresponding positions mentioned above, respectively. Using this equation in combination with numerical simulations at different locations, the capture efficiency of a single charged droplet can be fitted to calculate the capture of particulate matter.

The effect of particle sphericity on the capture efficiency is investigated by fitting the collision probability to the capture efficiency, using a model of spherical particles and non-spherical particles of different sphericity of the same volume and varying parameters such as particle size, particle charge, droplet charge, and particle motion velocity to investigate their effect on the capture efficiency and the positive and negative correlation with particle shape.

2.3. Solving Algorithm

Simulation studies are carried out to validate the computational models by building them and determining the physical parameters and boundary conditions. Simulation studies are then carried out first to investigate the collision probability of trapped micron particles. The trapping efficiency of submicron particles is then explored. The effects of particle size, droplet charge, and particle motion velocity are also discussed, and methods to improve the trapping efficiency are analyzed.

The fluid in the simulation is air, the simulation temperature is room temperature, The physical parameters are shown in Table 2 and the particle density is set to 2200 kg/m^3. The model inlet condition is a velocity–inlet boundary. The flow at the outlet is assumed to be fully developed and the model outlet boundary condition is the outflow boundary. A standard k-ω turbulence model is selected and the SIMPLE algorithm is chosen as the method for coupling pressure and velocity.

Table 2. Simulated air physical properties parameters [44].

Materials	Pressure (Mpa)	Temperature (°C)	Density (kg/m^3)	Viscosity Factor (Pa·s)
(air)	0	26.75	1.225	1.79×10^{-5}

2.4. Model Building and Validation

The commercial finite volume software ANSYS FLUENT 18.0 was used to solve the 3D Navier–Stokes equations and the particle equations of motion directly, with the computational domain shown in Figure 4. The single spherical droplet is fixed in the computational domain, and the droplet boundary is a wall boundary condition without considering the variation of the physical and chemical properties of the droplet. The air is fed from the left side of the computational domain in the plane (y–z), and the flow direction is the same as the x-axis. The particles are fed uniformly from the projection of the droplet on the inlet plane. Three hundred particles are fed at once, and the droplet diameter is taken to be 250 μm. The particle charge is set to 7.89E–17C, the particle velocity is set to 1.1 m/s, the electrostatic force is compiled and imported using UDF, and the particle motion and position are tracked using the DPM model. After each particle is tracked, the number of particles deposited onto the droplet (divided by the number of particles flowing since it is the capture efficiency) and the deposition position are counted.

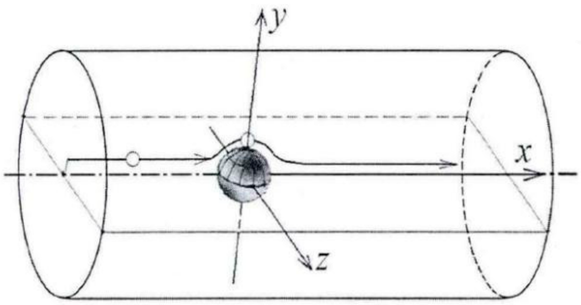

Figure 4. Geometry of the calculation area.

Considering the characteristics of the droplet boundary layer and the influence on the trajectory of the particles, the grid around the droplet was treated in an encrypted manner when dividing the grid, with a minimum grid of 9.4×10^{-13} m^3; see Figure 5.

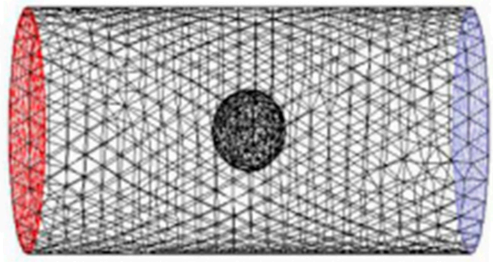

Figure 5. Grid division.

3. Results and Discussion

3.1. Effect of Particle Sphericity on Trapping Efficiency

A preliminary investigation was first carried out to obtain the effect of sphericity on droplet trapping micron particle trapping efficiency by investigating the effect of different particle sphericity on particle collision probability. Particles with sphericity of 0.1, 0.2, 0.3, 0.4, 0.5, 0.6, 0.7, 0.8, 0.9, and 1 were taken to simulate the collision probability of particles with different sphericity. The particle motion velocity was set at 1.1 m/s. Two particle sizes, 1.37 μm and 3.50 μm, were chosen for the simulations, and the results are shown in Figure 6.

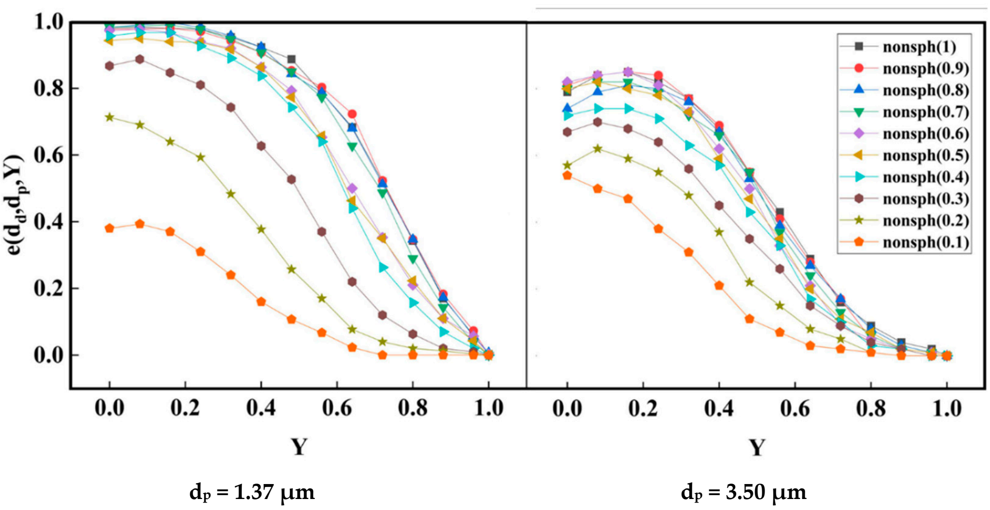

Figure 6. Collision probabilities at different sphericity values.

Analysis of Figure 6 shows that for particles of 1.37 μm, the collision probability is similar for sphericity of 0.6–1, with a significant reduction in particle impact on droplets occurring below 0.5. For particles of 3.50 μm, the difference in collision probability is slight. It overlaps more for sphericity of 0.5–1. Still, the difference in collision probability occurs at a sphericity of 0.4 or less, and particles of size 3.50 μm have a greater collision probability than particles of 1.37 μm under the same conditions. The analysis shows that particle sphericity affects the collision probability, and the effect is more significant for smaller particles. For both the 1.37 μm and 3.50 μm particle sizes, the probability of collision with a droplet decreases as the particle sphericity decreases. It can be assumed that particle shape affects the capture efficiency and that the more complex the particle shape, the lower the capture efficiency of single droplet capture particles.

3.2. Effect of Particle Size on Trapping Efficiency

For simple spherical micron particles, different particle sizes mainly affect their collision behavior, so the effect of particle size on collision probability is explored. Thus its effect on the trapping efficiency is analyzed. From the results in Figure 7a, it can be seen that particle size has a significant effect on the collision probability. As the particle size increases, the collision probability between the particle and the droplet also increases, and the collision efficiency for the 5.49 μm particles can reach 100%. As the particle release position gradually moves away from the droplet center, the particle–droplet collision probability decreases, reducing the capture efficiency.

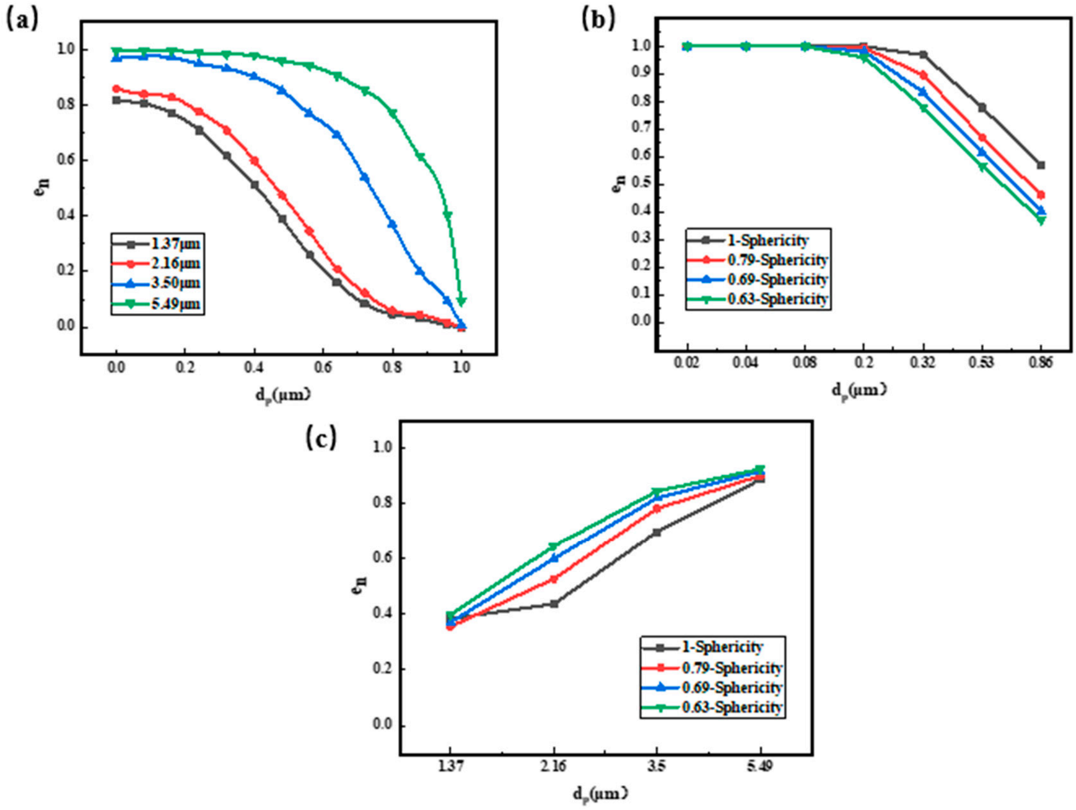

Figure 7. Trapping efficiency for different particle sizes (The sphericity is (**a**) 1 (**b**) 0.79 (**c**) 0.63).

For more complex, non-spherical particles, there is a positive correlation between size, charge, and capture efficiency. The four-micron particles of 1.37 μm, 2.16 μm, 3.50 μm, and 5.49 μm and seven submicron particles of 0.02 μm, 0.04 μm, 0.08 μm, 0.20 μm, 0.32 μm, 0.53 μm, and 0.86 μm given above were used to form linearly arranged aggregates of sphericity 1, 0.79, 0.69, and 0.63, respectively. The aggregates were formed with the sphericity of 1, 0.79, 0.69, and 0.63, respectively. The results in Figure 7b show that the trapping efficiency of the smaller non-spherical particles aggregated at 1.37 μm is less affected by aggregation behavior and mainly by electrostatic force. The larger non-spherical particles aggregated at 5.49 μm do not clearly show the effect of aggregation behavior because the non-spherical particles have a more significant inertial force and the trapping force affected by the particle shape is more diminutive. The electrostatic force mainly affects the non-spherical particles aggregated at 2.16 μm and 3.50 μm. The aggregation behavior of spherical particles with a size of 2.16 μm had the most significant effect on the capture efficiency, with an increase of around 25% at a sphericity of 0.79 and around 62.5% at a sphericity of 0.63. Although non-sphericality reduces the capture efficiency, the charge and size of the particles increase as they aggregate, which contributes to the increase in capture efficiency. The results in Figure 7c show that the capture efficiency of submicron spherical particles decreases as the particle size increases. The trapping efficiency is high for smaller-sized submicron particles, which are subject to less traction, and the non-spherical particles under this condition are mainly subject to electrostatic forces. At this point, the particles are primarily deposited towards the droplet surface, so the trapping efficiency is high. As the degree of particle aggregation increases, the effect of traction is more pronounced than the effect of inertia, and the trapping efficiency decreases.

3.3. Effect of Droplet Charge on Trapping Efficiency

For non-spherical particles, the droplet charge also affects the efficiency of droplet capture of particles. Droplets with charges of 3.95E–13C, 2.36E–13C, 1.38E–13C, and 6.78E–14C and non-spherical micron particles with the sphericity of 0.79 and 0.69, respectively, were selected for the simulations, and the results are shown in Figure 8a. The efficiency of droplet trapping of particles varies significantly with the droplet charge when the particle charge is a certain amount. As the droplet charge increases, the electrostatic force on the particles increases, the particles are pulled towards the droplet, and the efficiency of trapping non-spherical particles increases significantly. As the electrostatic forces on the particles are relatively smaller than the inertial and traction forces on the particles, the main parameter influencing the capture efficiency, in this case, is the particle size. For the same "equivalent diameter," the efficiency of trapping non-spherical particles is smaller than that of trapping spherical particles. For non-spherical particles formed by aggregation of submicron particles, the electrostatic force on the particles increases as the droplet charge increases for a given particle charge, making it easier for a droplet with a higher charge to trap more particles. When the droplet charge is 0C and 3.95E–13C, the capture efficiency is not affected by the aggregation behavior of the particles because the electrostatic force on the particles is 0. At a droplet charge of 3.95E–13C, the submicron particles are mainly affected by the electrostatic force and are less affected by the aggregation behavior of the particles. Analysis of Figure 8b, for the non-spherical particles formed by the aggregation of 0.20 μm spherical particles, shows a different trend when the non-spherical particles are four-particle aggregates, which is due to the larger particle inertial forces at this point coming into play. Analysis of Figure 8c shows that when the particle size is large enough, the particle traction force plays a significant role in trapping. The particle aggregation behavior still affects the trapping efficiency. In contrast, at a droplet charge of 0C, the submicron particles do not affect the trapping efficiency during aggregation due to their small size and low inertial forces. For submicron particles, the trapping efficiency decreases as the degree of particle aggregation increases.

3.4. Effect of Particle Motion Velocity on Trapping Efficiency

For spherical micron particles, the velocities of the above four different sizes of particles were selected as 0.3 m/s, 0.5 m/s, 0.8 m/s, 1.0 m/s, 1.1 m/s, 1.2 m/s, 1.5 m/s, 1.8 m/s, etc. The droplet charge was taken as 3.95E–13C, and the particle charge was taken as 7.89E–17C for the effect of particle motion velocity on the collision efficiency. In turn, its effect on the trapping efficiency was obtained, and the results are shown in Figure 9. When the particle velocity is small, the time the particle spends impacting the droplet is also long. At this time, the particle is subjected to less traction, accompanied by electrostatic force attraction, inertia force, and impact on the droplet. As can be seen from Figure 9a, the probability of collision for particles of size 1.37 μm is close to 100% when the velocity of motion is 0.3 m/s and 0.5 m/s. The impact of particle release position on the collision efficiency is almost non-existent. In contrast, for particles of larger size 5.49 μm, the analysis in Figure 9b shows that the collision probability changes as the particle release position changes.

(**a**) (**b**)

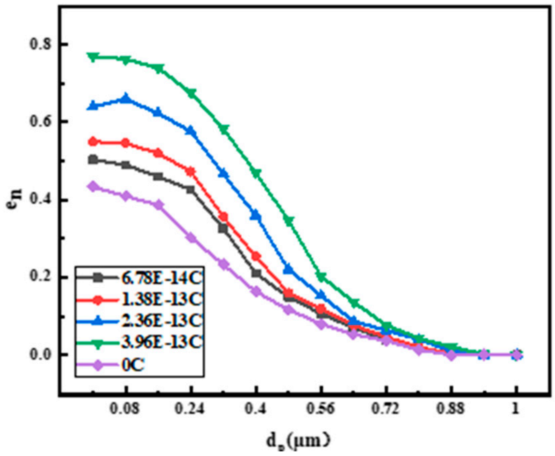

d_P = 1.37 μm

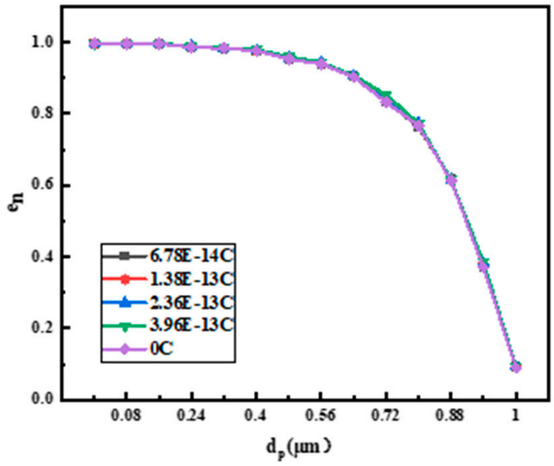

d_P = 3.50 μm

(**c**)

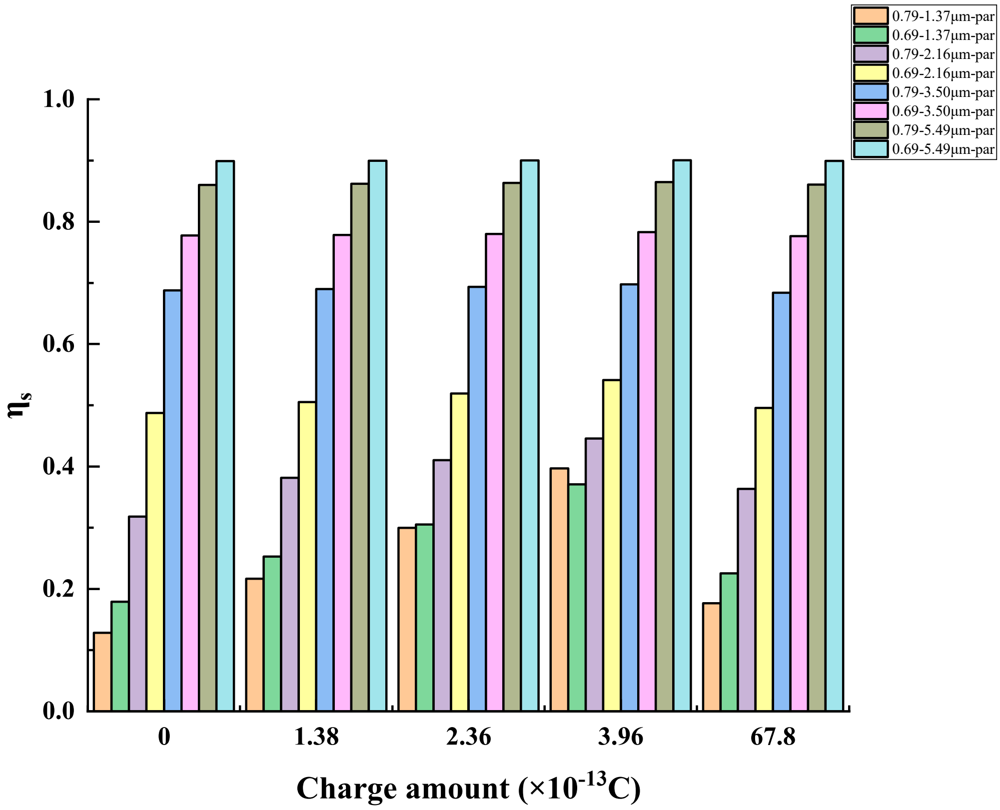

Figure 8. Trapping efficiency for different droplet charges.((**a**) micron particles (**b**) micron particles (**c**) submicron particles).

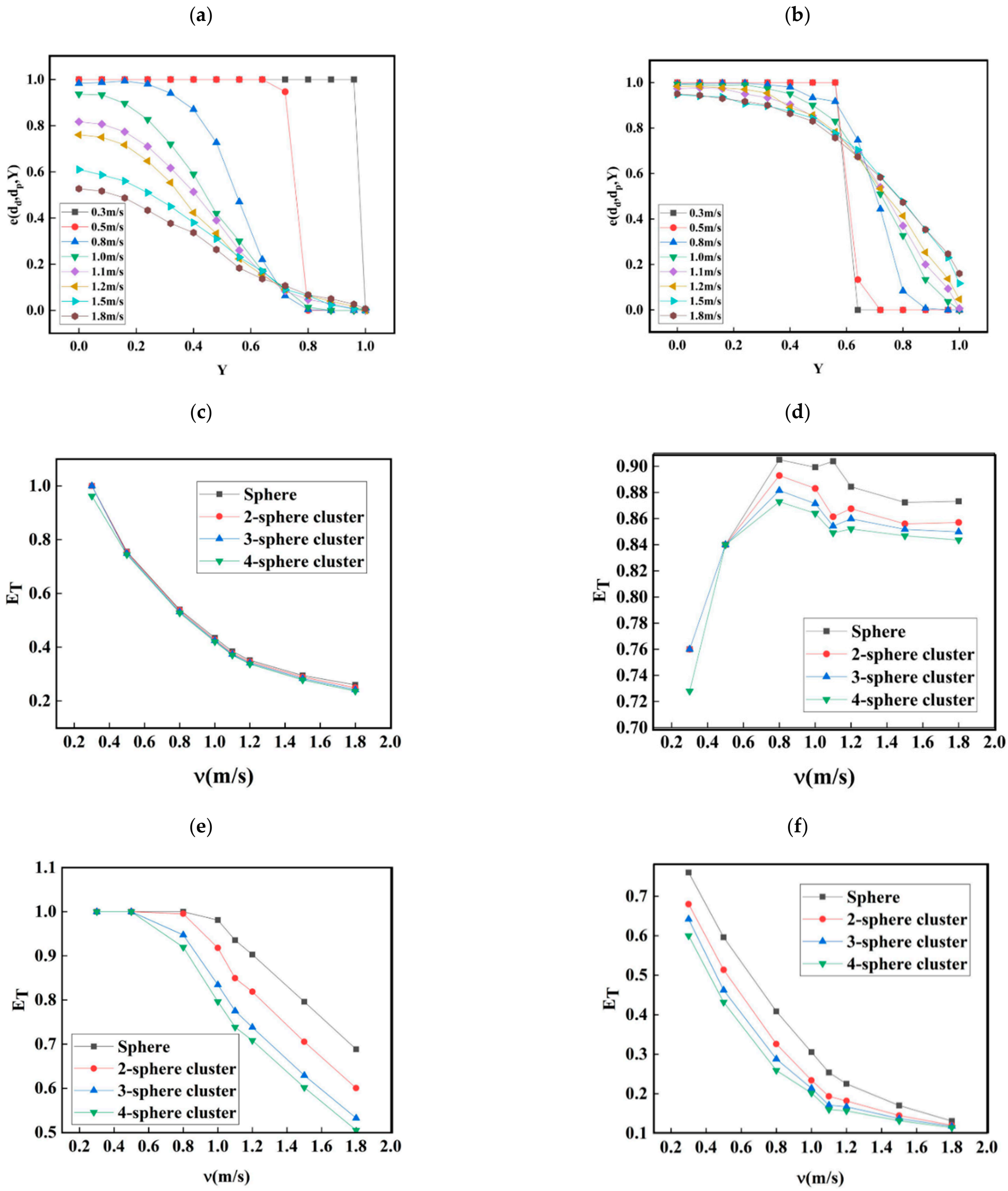

Figure 9. Trapping efficiency for different particle motion velocities ((**a**) 0.3 m/s, (**b**) 0.5 m/s, (**c**) 0.8 m/s, (**d**) 1.0 m/s, (**e**) 1.1 m/s, (**f**) 1.2 m/s).

For non-spherical particles, four different sizes and shapes of micron particles and submicron particle aggregates were selected above, and the velocities were set to 0.3 m/s, 0.5 m/s, 0.8 m/s, 1.0 m/s, 1.1 m/s, 1.2 m/s, 1.5 m/s, 1.8 m/s, etc. The droplet charge was set to 3.95E–13C, and the particle charge was set to 7.89E–17C for the simulation, and the results are shown in Figure 9c. For smaller micron particles of size 1.37 μm, the electrostatic force plays a dominant role when the velocity is small, and the droplets mostly trap the particles along with the electrostatic attraction, so their trapping efficiency is high. When the velocity of particle movement increases, the traction force also increases, which makes the particles deviate from the trajectory, and the trapping efficiency of non-spherical particles decreases. As seen from Figure 9d, for larger particles such as 5.49 μm, the effect of the electrostatic force is not obvious. The inertia force plays a dominant role when the particle motion speed is low, causing some particle motion trajectories to deviate from the droplet direction, leading to a decrease in the capture efficiency. As the velocity of particle motion increases, the trapping force on the particles increases, and the efficiency of non-spherical particles hitting the droplet increases under the combined effect of the forces on the particles. For particles of 1.37 µm size, the effect of particle shape is nearly absent. However, for particles of 5.49 µm size, the efficiency of capturing non-spherical particles is less than that of capturing spherical particles for the same "equivalent diameter." For non-spherical particles formed by aggregation of submicron particles of 0.08 µm, the electrostatic force plays a dominant role when the velocity is small. The droplets mostly trap the particles along with the electrostatic attraction. The trapping efficiency is not affected by the aggregation behavior of the particles when the velocity is 0.3 m/s and 0.5 m/s.

When the velocity of particle movement gradually increases, the particle is subjected to increased traction, making the particle gradually deviate from the trajectory. The efficiency of trapping non-spherical particles decreases, and the higher the degree of aggregation, the lower the trapping efficiency. The analysis in Figure 9e shows that the non-spherical particles formed by the aggregation of spherical particles of 0.20 µm are not affected by the aggregation behavior when the velocity is 0.3 m/s. However, as the velocity increases, the traction force on the non-spherical particles increases, and the efficiency of the non-spherical particles hitting the droplets decreases. The higher the degree of aggregation, the lower the trapping efficiency. As can be seen from Figure 9f, the aggregation of spherical particles of size 0.53 µm forms non-spherical particles because of the larger particle size, and the particles are subject to greater inertial forces and traction forces, so the aggregation behavior of particles has an impact on the capture efficiency, and the higher the degree of aggregation, the lower the capture efficiency. At an enormous particle movement speed, around 1.8 m/s, when the inertial force is more significant, particle aggregation behavior does not affect the capture efficiency. For non-spherical particles formed by the aggregation of 0.86 µm spherical particles, the effect on the trapping efficiency at 1.2 m/s is mainly absent; with the higher the degree of aggregation, the lower the trapping efficiency until then, after which the higher the degree of aggregation, the higher the trapping efficiency is demonstrated. At lower velocities, the capture efficiency is more significant for non-spherical particles with simpler aggregation patterns. When the velocity increases, the capture efficiency is smaller for non-spherical particles with more complex aggregation patterns, and the capture efficiency decreases as the particle aggregation increases.

4. Conclusions

(1) Using the standard k-ω turbulence model and SIMPLE algorithm, the trapping efficiency of charged droplets is positively correlated with the sphericity and the amount of charge. For micron particles, the efficiency of capturing spherical particles is greater than that of capturing non-spherical particles of equal volume. The aggregation behavior of submicron particles with low gravity is not conducive to the improvement of capture efficiency, and the capture efficiency can be reduced by up to 21.1% when non-spherical particles with a sphericity of 0.636 are formed.

(2) Particle size has a significant effect on the capture efficiency, increasing size increases the capture efficiency, and the effect of particle velocity on the capture efficiency needs to be considered in conjunction with particle size. Particle size less than or equal to 2.16 µm has a higher capture efficiency in the range of particle motion velocity less than 0.5 m/s. In comparison, particle size greater than or equal to 3.50 µm has a higher capture efficiency in the range of particle motion velocity greater than 0.8/s.

(3) Increasing the charge of particles and droplets could increase the Coulomb force on particles and improve the trapping efficiency of particles; as the gravity of submicron particles is minimal, the aggregation behavior is not conducive to the improvement of

trapping efficiency, and the trapping efficiency can be reduced by up to 21.1% when tetramers are formed.

Author Contributions: Conceptualization, Q.S. and J.G.; data curation, W.Z.; investigation, Q.S. and Y.D.; methodology, H.D.; project administration, Y.Z. and J.W.; visualization, Q.D.; writing—original draft, W.Z.; writing—review & editing, Y.Z. All authors have read and agreed to the published version of the manuscript.

Funding: This work was supported by the National Natural Science Foundation of China (52006047) and the National Key Research and Development Program of China (Gas Boiler Energy Efficiency Emission Online Inspection and Intelligent Diagnosis Platform Development 2021YFF0600605).

Conflicts of Interest: The authors declare no conflict of interest.

References

1. Luo, R.S.; Wei-Quan, Y.U.; Lin, G.X.; Cheng, G.H.; Chen, Y.C.; Lin, X.; Zheng, Y.F. Analysis on Reform of Wet ESP Technology Utilized in 700MW Generating Set of Power Plant. *China Environ. Prot. Ind.* **2018**, 110–116.
2. Liu, X.; Xu, Y.; Zeng, X.; Zhang, Y.; Xu, M.; Pan, S.; Zhang, K.; Li, L.; Gao, X. Field Measurements on the Emission and Removal of PM2.5 from Coal-Fired Power Stations: 1. Case Study for a 1000 MW Ultrasupercritical Utility Boiler. *Energy Fuels* **2016**, *30*, 6547–6554. [CrossRef]
3. Pettersson, J.; Andersson, S.; Bafver, L.; Strand, M. Investigation of the Collection Efficiency of a Wet Electrostatic Precipitator at a Municipal Solid Waste-Fueled Combined Heat and Power Plant Using Various Measuring Methods. *Energy Fuels* **2019**, *33*, 5282–5292. [CrossRef]
4. Jiang, S.; Feng, H.; Jxa, B.; Hu, Y.B.; Zga, B.; Xl, C. Exploring the influences of Li_2O/SiO_2 ratio on Li_2O—Al_2O_3—SiO_2—B_2O_3—BaO glass-ceramic bonds for vitrified cBN abrasives. *Ceram. Int.* **2019**, *45*, 15358–15365.
5. Yao, J.; Wu, J.; Zhao, Y.; Lim, E.; Cao, P.; Fang, Z.; Wang, C.H. Experimental investigations of granular shape effects on the generation of electrostatic charge. *Particuology* **2018**, *15*, 82–89. [CrossRef]
6. Pendar, M.R.; Pascoa, J. Numerical Simulation of the Electrostatic Coating Process: The Effect of Applied Voltage, Droplet Charge and Size on the Coating Efficiency. *SAE Int. J. Adv. Curr. Pract. Mobil.* **2021**, *22*, 189–205.
7. Wadell, H. The Coefficient of Resistance as a Function of Reynolds Number for Solids of Various Shapes. *J. Frankl. Inst.* **1934**, *217*, 459–490. [CrossRef]
8. Yan, Z.X. Experimental Study of the Effect of Chemical Coagulation on the Performance of a Wet Type Electric Precipitator. Master's Thesis, Yanshan University, Qinhuangdao, China, 2021.
9. Ziwen, Z.; Junfeng, W.; Yuanping, H. Study of the particle trapping characteristics of charged droplets. *J. Eng. Thermophys.* **2018**, *39*, 355–360.
10. Cui, R.; Liu, H.; Gao, H.; Gao, Z. Research status and prospect of abatement of ultrafine particles in flue gas. *China Energy Environ. Prot.* **2018**, *40*, 123–126.
11. Liying, S. Experimental Study on the Charging Performance of Water Mist and Its Dust Reduction Effect. Masters' Thesis, Liaoning University of Engineering and Technology, Liaoning, China, 2019.
12. Yao, G.M.; Wei, B.; Ren, Y.C. Numerical simulation of charged droplets trapping particles. *Energy Conserv.* **2015**, *11*, 41–44.
13. Wen, Z.Y. Experimental Study on the Removal of Fine Particulate Matter from an Electrostatic Spray Cyclone Dust Collector. Master's Thesis, Jiangsu University, Jiangsu, China, 2017.
14. Geng, P.; Zore, A.; Van De Mark, M.R. Thermodynamic Characterization of Free and Surface Water of Colloidal Unimolecular Polymer (CUP) Particles Utilizing DSC. *Polymers* **2020**, *12*, 1417. [CrossRef] [PubMed]
15. Wang, P.K. Collection of aerosol particles by a conducting sphere in an external electric field—Continuum regime approximation. *J. Colloid Interface Sci.* **1983**, *94*, 301–318. [CrossRef]
16. Shapiro, M.; Laufer, G. The effect of electrostatic field direction on the diffusion of charged dust particles from the flowstream to a sphere. *J. Colloid Interface Sci.* **1984**, *99*, 256–269. [CrossRef]
17. Junfeng, W.; Liyu, X.; Yuanping, H. Effect of droplet deformation on the adsorption of fine particles by charged water mists. *Chin. Sci. Technol. Pap.* **2015**, *10*, 1303–1308.
18. Junfeng, W.; Jin, L.; Huibin, X. Advances in wet desulphurisation for the synergistic removal of fine particulate matter. *Chem. Prog.* **2019**, *38*, 3402–3411.
19. Su, L.; Zhang, Y.; Du, Q.; Dai, X.; Wang, H. An experimental study on the removal of submicron fly ash and black carbon in a gravitational wet scrubber with electrostatic enhancement. *RSC Adv.* **2020**, *10*, 5905–5912. [CrossRef]
20. Zhao, H.B.; Zheng, C.G. Operation Optimization of Electrostatically Enhanced Wet Scrubbers. *J. Power Eng.* **2007**, *27*, 954–959.
21. Li, H.; Zhang, M.; Zhu, L.; Yang, J. Stability of mercury on a novel mineral sulfide sorbent used for efficient mercury removal from coal combustion flue gas. *Environ. Sci. Pollut. Res.* **2018**, *25*, 28583–28593. [CrossRef]
22. Ao, W. Study of the Behaviour and Mechanism of Single Droplet Trapping of Fine Particles. Ph.D. Thesis, Tsinghua University, Beijing, China, 2016.

23. Chang, H.J.; Yong, P.K.; Lee, K.W. A moment model for simulating raindrop scavenging of aerosols. *J. Aerosol Sci.* **2003**, *34*, 1217–1233.
24. Feng, D.; Shang, Q.; Dong, H.; Zhang, Y.; Wang, Z.; Li, D.; Xie, M.; Wei, Q.; Zhao, Y.; Sun, S. Catalytic mechanism of Na on coal pyrolysis-derived carbon black formation: Experiment and DFT simulation. *Fuel Process. Technol.* **2021**, *224*, 107011. [CrossRef]
25. Slinn, W.G.N. Some approximations of the wet and dry removal of particles and gases from the atmosphere. *Water Air Soil Pollut.* **1977**, *7*, 513–543. [CrossRef]
26. Davenport, H.M.; Peters†, L. Field studies of atmospheric particulate concentration changes during precipitation. *Atmos. Environ.* **1978**, *12*, 997–1008. [CrossRef]
27. Weber, M.E.; Paddock, D. Interceptional and gravitational collision efficiencies for single collectors at intermediate Reynolds numbers. *J. Colloid Interface Sci.* **1983**, *94*, 328–335. [CrossRef]
28. Bauer, S.E.; Bausch, A.; Nazarenko, L.; Tsigaridis, K.; Xu, B.; Edwards, R.; Bisiaux, M.; Mcconnell, J. Historical and future black carbon deposition on the three ice caps: Ice core measurements and model simulations from 1850 to 2100. *J. Geophys. Res. Atmos.* **2013**, *118*, 7948–7961. [CrossRef]
29. Horn, H.G.; Bonka, H.; Gerhards, E.; Hieronimus, B.; Kalinowski, M.; Kranz, L.; Maqua, M. Collection efficiency of aerosol particles by raindrops. *J. Aerosol Sci.* **1988**, *19*, 855–858. [CrossRef]
30. Loth, E. Drag of non-spherical solid particles of regular and irregular shape. *Powder Technol.* **2008**, *182*, 342–353. [CrossRef]
31. Ma, L.; Qin, C.; Pi, S.; Cui, H. Fabrication of efficient and stable Li_4SiO_4-based sorbent pellets via extrusion-spheronization for cyclic CO_2 capture. *Chem. Eng. J.* **2020**, *379*, 122385. [CrossRef]
32. Nedelcu, D.; Iancu, V.; Gillich, G.R.; Bogdan, S.L. Study on the effect of the friction coefficient on the response of structures isolated with friction pendulums. *Vibroeng. Procedia* **2018**, *19*, 6–11. [CrossRef]
33. Leal, L.G. Bubbles, drops and particles. *Int. J. Multiph. Flow* **1979**, *5*, 229–230. [CrossRef]
34. Dallavalle, J.M. *Micrometrics*; Pitman Publishing: New York, NY, USA, 1948; pp. 55–60.
35. White, F.M. *Fluid Mechanics*; McGraw-Hill: New York, NY, USA, 1991.
36. Feng, D.; Zhao, Y.; Zhang, Y.; Xu, H.; Zhang, L.; Sun, S. Catalytic mechanism of ion-exchanging alkali and alkaline earth metallic species on biochar reactivity during CO_2/H_2O gasification. *Fuel* **2018**, *212*, 523–532. [CrossRef]
37. Schiller, L. Uber die grundlegenden Berechungen bei der Schwerkraftaufbereitung. *Z. Ver. Dtsch. Inge* **1933**, *77*, 318–321.
38. Clift, R.; Gauvin, W. The motion of particles in turbulent gas streams. *Rev. Argent. Cardiol.* **1970**, *82*, 14–28.
39. Dressel, M. Dynamic Shape Factors for Particle Shape Characterization. *Part. Part. Syst. Charact.* **1985**, *2*, 62–66. [CrossRef]
40. Feng, D.; Zhang, Y.; Zhao, Y.; Sun, S.; Wu, J.; Tan, H. Mechanism of in-situ dynamic catalysis and selective deactivation of H2O-activated biochar for biomass tar reforming. *Fuel* **2020**, *279*, 118450. [CrossRef]
41. Leith, D. Drag on Nonspherical Objects. *Aerosol Sci. Technol.* **1987**, *6*, 153–161. [CrossRef]
42. Ganser, G.H. A rational approach to drag prediction of spherical and nonspherical particles. *Powder Technol.* **1993**, *77*, 143–152. [CrossRef]
43. Lu, X. Conservation of Energy, Entropy Identity, and Local Stability for the Spatially Homogeneous Boltzmann Equation. *J. Stat. Phys.* **1999**, *96*, 765–796. [CrossRef]
44. Dai, X. Wet Electrocoagulation and Removal of Fine Particulate Matter from Coal Combustion. Master's Thesis, Harbin Institute of Technology, Harbin, China, 2018.
45. Fengqiao, H.; Yanming, K.; Ke, Z. Influence of turbulence effects on particle trapping processes on raindrop surfaces. *China Environ. Sci.* **2017**, *37*, 13–20.